KRONOS FUSION ENERGY

PAPER 2.98 · THE KRONOS 2026 SERIES

Two-Code Cross-Validation of Negative-Triangularity Turbulence Suppression in a Compact Spherical-Tokamak Breeder: Quasilinear TGLF Confirms Nonlinear CGYRO

The Hyperion breeder stakes its confinement on a single physics choice: that strong negative triangularity () places the plasma core in a quiet, subcritical turbulence basin. A...

Read it live — 3-D model · physics validator · film series

BY P I FORD

2026 · EDITORIAL EDITION

THE OFFICIAL RECORD

What this document is, and how to read its numbers

This is a combined editorial. It gathers, in one volume, the two design studies Kronos Fusion Energy released in 2026 — a compact spherical-tokamak tritium/helium-3 breeder and a deuterium–helium-3 tandem-mirror generator — together with the intellectual-property estate, the people, and, in the internal edition, the full commercial case. The scientific text is the same text that appears in the arXiv preprints and the journal submissions; the editorial adds the apparatus a reader needs to hold the whole program at once, and nothing in the physics is altered to fit it.

THE HONESTY STANCE IS THE ASSET

Every headline quantity carries an **evidence class** — DERIVED RECOMPUTED MEASURED REQUIREMENT — and, where a number is a modelled extrapolation rather than a demonstrated value, it is labelled as such and its downside is shown next to it. Several quantities in the underlying corpus moved after first publication; where a value has been withdrawn or restated, the record says so plainly. This is deliberate: a diligence team will find the load-bearing assumptions, so the document surfaces them first.

TWO EDITIONS

This volume is issued in two editions. The **public edition** (light) carries the physics and the design only — no dollar, price, or per-kilogram figure appears anywhere in it. The **internal edition** (dark) adds the economics, the funding architecture, and the defense-commercial analysis, and is marked *Confidential* accordingly; it is not for public distribution. Where the commercial case rests on a modelled assumption rather than a demonstrated one, it is labelled as such and its downside is shown alongside it, on the same terms as the physics.

TITLE	The Kronos Fleet — Hyperion · Aegis · MetroVolt: A Combined Design & Commercialization Study
AUTHOR	Priyanca Ford, Founder & CEO, on behalf of Kronos Fusion Energy
EDITION	2026 Combined Editorial · first issue
COMPANION WORKS	The five-paper arXiv drop — (1) Breeder, (2) Burner, (3) REBCO magnet & tape, (4) Direct Energy Conversion, (5) AI/ML/Quantum control — with matching numbered Zenodo deposits, plus the IOP journal and IAEA-FEC submissions. Patents were filed before the drop.
NAMING	Hyperion = the breeder; Aegis (defense) and MetroVolt (data-center) = one generator in two housings. Internal mode letters (D1, L) do not appear on public surfaces.
STATUS	Conceptual design & simulation study. Nothing herein is a construction commitment.

HOW TO READ THIS VOLUME

The fleet at a glance, and the way its numbers are marked

This volume opens with *Orientation*, presents the five research papers as a bound sequence, and closes with the *Apparatus*. *Foundations* sets out the three general results both machines rest on. *Paper One* is the Hyperion breeder; *Paper Two* the Aegis / MetroVolt generator; *Papers Three, Four and Five* are the enabling science — high-field REBCO magnets and tape, direct energy conversion, and the AI / ML / quantum control stack. A *Digital Twin & 3-D Model* part follows, then the *Environmental* profile. The *Economics* and levelized cost and the *Business Case* and diligence record appear in the internal edition only; the *Simulations* proof record and the Apparatus — patent portfolio, team, limitations, and sources — close both editions.

THE FLEET AT A GLANCE

	HYPERION	AEGIS	METROVOLT
Role	Strategic-isotope foundry	Defense installation power	Campus power
Machine	**Spherical tokamak**	**Tandem mirror**	**Tandem mirror**
Fuel	Deuterium–tritium	Deuterium–helium-3	Deuterium–helium-3
Delivers	Tritium · ^{3}He · 14 MeV n	Resilient installation power	Firm campus power
Physics bar	**Fusion gain only**	Closure (gates named)	Closure + lunar ^{3}He
In the fleet	Breeds the fuel	Proves the generator	Commercial destination

HOW THE NUMBERS ARE MARKED

Every headline quantity carries an evidence class — DERIVED from first principles, RECOMPUTED from raw data, MEASURED in hardware, or a REQUIREMENT yet to be met. Financial figures carry a case label and are confined to the internal (confidential) edition. Values that moved after first publication are shown as withdrawn or restated rather than quietly changed. A capability you can evaluate is one whose limits are on the page.

ABSTRACT

Two-Code Cross-Validation of Negative-Triangularity Turbulence Suppression in a Compact Spherical-Tokamak Breeder: Quasilinear TGLF Confirms Nonlinear CGYRO

The Hyperion breeder stakes its confinement on a single physics choice: that strong negative triangularity ($\delta = -0.30$) places the plasma core in a quiet, subcritical turbulence basin. A claim of that weight must not rest on one code. Here we cross-validate the claim with two independent members of the GACODE family evaluated on the identical frozen design case (config-22021: $R_0 = 1.20\,m$, $a = 0.48\,m$, $\kappa = 2.0$, $\delta = -0.30$, $B_0 = 8\,T$, $q_{95} = 3.0$, at the negative-triangularity anchor $Q = 3.076$, $I_p = 9.66\,MA$). The high-fidelity nonlinear code CGYRO, run at the real electron-to-ion mass ratio $\mu = 3672$ for the ion scale, returns a saturated gyro-Bohm heat flux of $Q = 37.2$ at negative triangularity against $Q = 64.2$ at positive triangularity — an ion-scale suppression of $\mathbf{38–42\,\%}$, inside the frozen design band — and a nonlinear electron-temperature-gradient (ETG) flux of $Q_e = 23.4$ against 110.7 at $a/L_{Te} = 3.0$, a $\mathbf{79–80\,\%}$ suppression; its cross-scale linear growth-rate spectrum is suppressed by $31–60\,\%$ at every resolved wavenumber $k_y = 0.1–6.0$. The fast quasilinear model TGLF, driven through the flux-matching transport solver TGYRO on the same equilibrium, reproduces the quiet basin and a flux-driven energy confinement of $\tau_E = 0.410\,s$ ($H_{98} \approx 0.94$). We cast the cross-validation as a formal agreement test on the suppression fraction and show the two codes agree on sign, magnitude and robustness: the advantage holds at $56–66\,\%$ across a factor-of-16 collisionality scan and survives kinetic electrons at finite β_e up to 0.010. The comparison is anchored to the byte: the stand-alone CGYRO linear reference returns $\gamma = +0.3179$ (a-units) byte-identically to its bundled benchmark. A fast quasilinear surrogate can therefore stand in for full nonlinear gyrokinetics inside the Kronos real-time control loop with a first-principles check behind it. All computation was performed on the NVIDIA GPU HPC campaign.

Open-access deposit (code & data, CC BY 4.0): DOI 10.5281/zenodo.22645864 · Zenodo community *kronos_fusion_energy*. Explore it live: interactive 3-D model · physics validator.

Keywords: gyrokinetics · CGYRO · TGLF · TGYRO · negative triangularity · turbulence suppression · two-code cross-validation · reproducibility · spherical-tokamak breeder

CONTENTS

Table of Contents

NOMENCLATURE

Symbols, units, and the names of things

Q	plasma (fusion) gain, P_{fus}/P_{aux}
Q_E	engineering gain, net electric out / recirculating in
H_{98}	confinement enhancement over the IPB98(y,2) scaling
Z_{eff}	effective ion charge
c_{ee}	electron–electron bremsstrahlung leading coefficient, 2.120022 (exact)
τ_E	energy confinement time
I_p	plasma current
R_0, a	major radius, minor radius
κ, δ	elongation, triangularity
β_N	normalized plasma beta (Troyon-normalized)
TBR	tritium breeding ratio
DEC	direct energy conversion
CF	plant capacity factor (availability)
FOAK / NOAK / BOAK	first / n^{th} / best of a kind
Hyperion	the ST breeder (internal: Mode D2)
Aegis	the generator, defense/installation housing (internal: Mode M)
MetroVolt	the generator, data-center housing (Mode M)

§ 1

Introduction

NEGATIVE TRIANGULARITY AS THE LOAD-BEARING DESIGN CHOICE

A spherical tokamak (ST) confines a large plasma current in a small volume, which is exactly what recommends it as a compact neutron source and tritium breeder [1,2] and, at the same time, what makes its transport physics unforgiving. The Hyperion breeder holds $I_p = 9.66\,MA$ at a major radius of only $R_0 = 1.20\,m$, at aspect ratio $A = 2.5$, behind a centrepost magnet at a peak field of 16.84 T, delivering $Q = 3.076$ and $P_{\text{fus}} = 85.04\,MW$. The confinement case for that operating point rests on one shaping decision: strong negative triangularity, $\delta = -0.30$. Negative triangularity accesses good core confinement without the edge pressure pedestal and the associated edge-localised-mode (ELM) cycle of conventional H-mode [3,4,5]; recent experiments have confirmed both the reduced core transport and the robust ELM-free edge on DIII-D and TCV [3,6]. The essential physics is that reversing the sign of the triangularity alters the local magnetic drift geometry so as to raise the critical gradient for ion-temperature-gradient (ITG) and trapped-electron-mode (TEM) turbulence, deepening a *quiet basin* of subcritical transport [4,7].

If the quiet basin is real, deep and robust, the breeder's confinement anchor is sound; if it is shallow, a collisionality artifact, or an ion-scale illusion that electron-scale turbulence erases, the design point is not supported. The Kronos programme has resolved the nonlinear physics of the basin in a companion paper [33] [doi:10.5281/zenodo.22645722; official page], which reports the nonlinear CGYRO ion- and electron-scale quiescence at the operating point. The present paper asks a different, methodological question, and it is the question that determines whether that physics can be trusted and whether it can be used online.

THE STANDARD OF PROOF: TWO CODES MUST AGREE

The accepted standard of proof in gyrokinetic transport is not a single well-converged run but agreement between two codes of different fidelity and different numerical construction. Two failure modes make single-code results fragile: an implementation error that a benchmark case would catch, and a modelling choice (mass ratio, collision operator, saturation rule) that biases the answer. The community has addressed both through cross-code verification — the Cyclone base case and its descendants [17], the GENE/GYRO/GS2 comparisons [18], and the general verification-and-validation programme for magnetic-fusion simulation [19,20]. The strongest form of the argument pairs a *reduced quasilinear* model, cheap enough to run inside a control loop, with a *first-principles nonlinear* simulation that is not: if the two predict the same effect on the same case, the reduced model can be trusted where the expensive one cannot run, and the physics can be trusted because it survived an independent method.

This is precisely the check the Hyperion confinement anchor requires, for two reasons. First, the design freeze must be defensible: a $\sim 40\,\%$ turbulence suppression that appears in one nonlinear code and nowhere else would not survive review. Second, the Kronos real-time digital twin runs a quasilinear transport surrogate inside its control loop [34] [doi:10.5281/zenodo.22645803; official page]; that surrogate is only trustworthy if the quasilinear physics it emulates has itself been checked against the nonlinear code it stands in for, on the case that matters.

CONTRIBUTION

This paper reports the two-code cross-validation of the negative-triangularity quiet basin. We use two codes from the GACODE family: TGLF, a saturation-rule quasilinear transport model [8,9] fast enough for real-time use, driven through the flux-matching transport solver TGYRO [12]; and CGYRO [10], a nonlinear (and linear) Eulerian gyrokinetic solver that is the high-fidelity reference. Both are applied to the identical frozen negative-triangularity design case, with positive-triangularity comparators built by reversing only the triangularity sign. Our specific contributions are:

a formal statement of the governing gyrokinetic problem, the Miller local-equilibrium parametrization of the shared case, the gyro-Bohm normalization, and the quasilinear closure, so that "the same case" has an unambiguous meaning across the two codes (§2);
a cross-validation acceptance criterion written as an inequality on the suppression fraction, and its numerical formulation — discretization, solver, convergence — for both codes (§2 and §3);
a dedicated account of the NVIDIA GPU HPC campaign that produced the results, including the codes run, the problem scale, and the byte-exact reproducibility of the linear reference (§3);
the cross-validated results: nonlinear ion- and electron-scale fluxes, the linear spectrum, the quasilinear confinement, and the robustness of the basin under collisionality and finite β (§4); and
a quantitative comparison to the published negative-triangularity and gyrokinetic-verification literature (§5). enumerate
Every quantitative claim traces to a frozen result in the Kronos Physics De-Risking Register [31]; the serial identifiers (e.g. BR-L2-A1c) are given inline so each number is auditable. The reference CGYRO data are archived as a permanent Kronos deposit [32].

§ 2

Governing equations and the formal problem

THE GYROKINETIC VLASOV–MAXWELL SYSTEM

Both codes solve the same underlying physics: the electromagnetic gyrokinetic Vlasov–Maxwell system in the δf formulation [10,11]. For each species s the perturbed gyrocentre distribution $\delta f_s(R, \varepsilon, \mu, t)$ evolves according to

$$\frac{\partial \delta f_s}{\partial t} + (v_\parallel \; b + \; v_{Ds} + \langle \; v_E\rangle)\cdot\nabla\delta f_s + \langle \; v_E\rangle\cdot\nabla F_{0s} - C_s[\delta f_s] = 0,$$

where $b = B/B$, F_{0s} is the local Maxwellian background, and the gyro-average $\langle\cdot\rangle$ is taken at fixed gyrocentre R. The two drifts that carry the turbulence are the magnetic drift

$$v_{Ds} = \frac{1}{\Omega_s}\left(v_\parallel^2 + \tfrac{1}{2}v_\perp^2\right) \quad b \times \left(\frac{\nabla B}{B} + \quad \kappa\right), \qquad \Omega_s = \frac{q_s B}{m_s},$$

with field-line curvature $\kappa = b\cdot\nabla \; b$, and the fluctuating $E \times B$ drift $\langle v_E\rangle = b \times \nabla\langle\chi\rangle/B$ derived from the gyrokinetic potential $\chi = \phi - v_\parallel A_\parallel + (\ldots)$. Equation (2) is the seat of the triangularity effect: ∇B and κ are set by the flux-surface shape, so changing δ changes the drive geometry that v_{Ds} imposes on equation (1). The collision operator C_s is the linearised Sugama multi-species operator [14] as implemented in CGYRO.

The fields close the system through the gyrokinetic field equations — quasineutrality for the electrostatic potential ϕ,

$$\sum_s q_s \int d^3v\,\left(\langle\delta f_s\rangle - \tfrac{q_s}{T_s}(\phi - \langle\phi\rangle)F_{0s}\right) = 0,$$

and the parallel and perpendicular Ampère laws for $A_\parallel$ and $\delta B_\parallel$, which are retained in the electromagnetic (finite-β) runs of §4. Equations (1)–(3) are integrated directly by CGYRO; TGLF solves the same eigenvalue problem in a reduced gyro-Landau-fluid moment truncation (§2.4).

THE SHARED CASE: MILLER LOCAL EQUILIBRIUM

So that “the same case” is unambiguous, both codes are evaluated on a local Miller equilibrium [15,16] extracted at mid-radius, $\rho = 0.6$, from the frozen breeder toolkit anchor config-22021 [BR-L2-A17]. The flux surface is parametrized by

$$R(\theta) = R_0 + r\cos\big(\theta + \arcsin\delta\,\sin\theta\big),$$
$$Z(\theta) = \kappa\, r\sin\theta,$$

with the local minor radius r, elongation κ, and triangularity δ, together with the radial gradients $\partial_r\kappa$, $\partial_r\delta$, the Shafranov shift $\partial_r R_0$, the safety factor q and the magnetic shear $\hat{s} = (r/q)\,\partial_r q$. The frozen geometry is $R_0 = 1.20\,m$, $a = 0.48\,m$, $\kappa = 2.0$, $B_0 = 8\,T$ and $q_{95} = 3.0$, with the shaping under test entering only through δ. The negative-triangularity case sets $\delta = -0.30$; the positive-triangularity comparator sets $\delta = +0.30$ with every other input — gradients, collisionality, β — held fixed (figure 1). This isolates the triangularity sign as the sole difference between the two branches, which is what makes the comparison a clean test of the shaping.

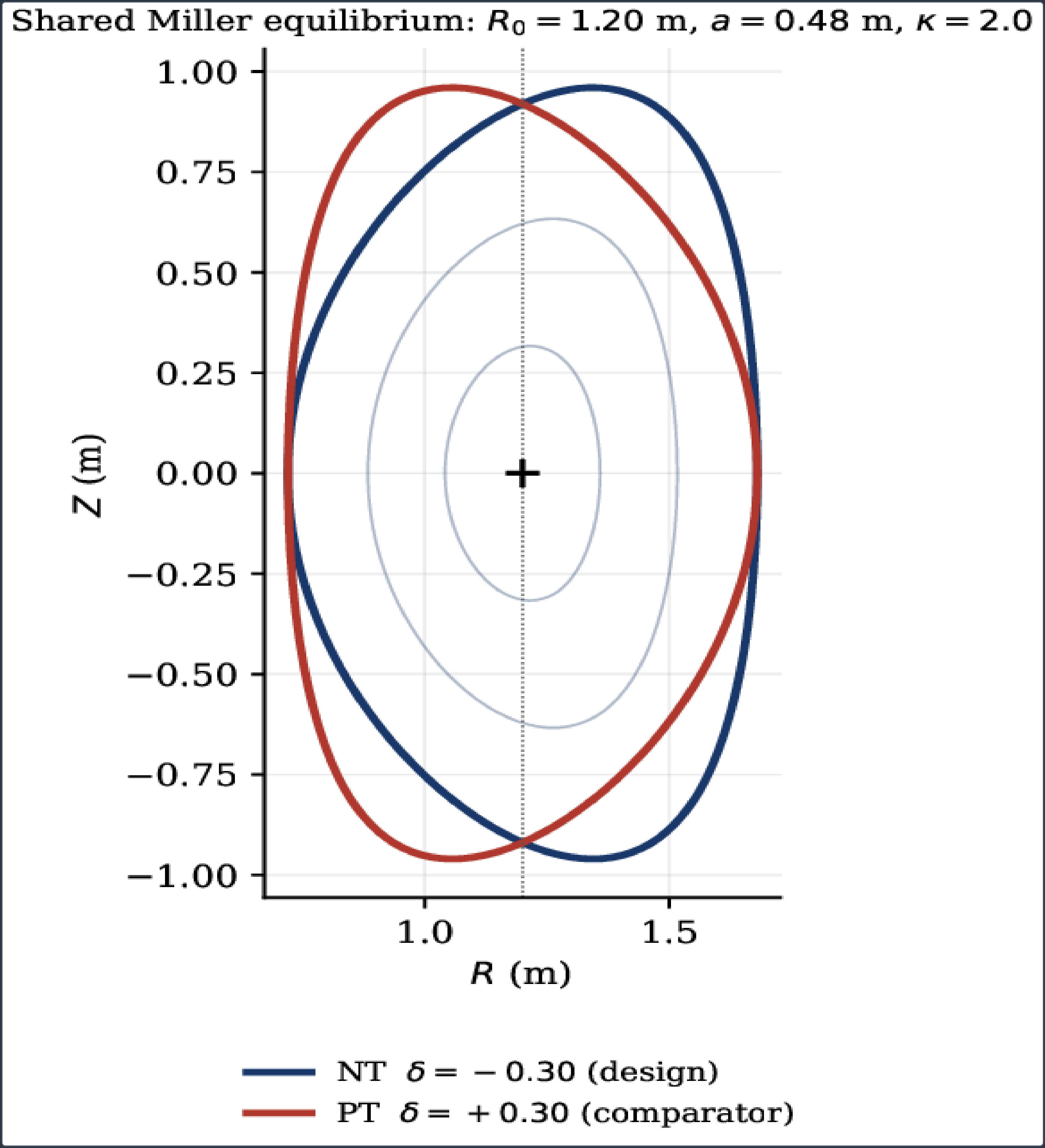

(Schematic.) The shared Miller local equilibrium of equations (4)–(4) at $R_0 = 1.20\,m$, $a = 0.48\,m$, $\kappa = 2.0$. The negative-triangularity design branch ($\delta = -0.30$, blue) and the positive-triangularity comparator ($\delta = +0.30$, red) differ only in the triangularity sign; faint inner curves indicate the nested surfaces of the design branch. Geometry only; no data values are shown (BR-L2-A17).

GYRO-BOHM NORMALIZATION AND THE HEAT FLUX

Turbulent fluxes are reported in gyro-Bohm units, the natural scale for local flux-tube gyrokinetics. With $c_s = \sqrt{T_e/m_i}$ the ion sound speed, $\rho_s = c_s/\Omega_i$ the sound gyroradius, and a the minor radius, the gyro-Bohm heat-flux unit is

$$Q_{\mathrm{GB}} = n_e\, T_e\, c_s \left(\frac{\rho_s}{a}\right)^2,$$

and the species heat flux carried by the turbulence is the flux-surface average of the fluctuating $E \times B$ energy flow,

$$Q_s = \left\langle \int d^3v \, \tfrac{1}{2} m_s v^2 \, \delta f_s \, (\langle v_E \rangle \cdot \nabla r) \right\rangle, \qquad Q \equiv Q_i / Q_{\mathrm{GB}}.$$

All fluxes Q, Q_e quoted below are in these units. The dimensionless drive is the normalized inverse gradient scale length $a/L_{Ts} = -\,a\,\partial_r \ln T_s$.

THE QUASILINEAR CLOSURE (TGLF)

TGLF replaces the direct nonlinear integration of equation (1) by a two-stage quasilinear model [8,9]. First it solves the linear gyrokinetic eigenvalue problem in a 15-moment gyro-Landau-fluid truncation, returning for each binormal wavenumber k_y a set of unstable eigenmodes with complex frequency $\omega_j(k_y) = \omega_{r,j} + i\gamma_j$ and eigenfunction $\hat{\phi}_j$. The turbulent flux is then the quasilinear weight of each mode multiplied by a saturated fluctuation intensity supplied by a saturation rule:

$$Q^{\mathrm{QL}} = \sum_{k_y} \sum_j \underbrace{\frac{\langle Q_j(k_y) \rangle}{\langle |\hat{\phi}_j(k_y)|^2 \rangle}}_{\text{quasilinear weight } W_j} \; |\hat{\phi}_j(k_y)|^2_{\mathrm{sat}},$$

where $|\hat{\phi}_j|^2_{\mathrm{sat}}$ follows the SAT saturation model, which encodes the nonlinear zonal-flow regulation of the mode amplitude calibrated to a nonlinear-gyrokinetic database. Equation (7) is orders of magnitude cheaper than integrating equation (1) directly, which is what makes TGLF admissible inside a control loop; the price is the modelling content of W_j and the saturation rule, and it is exactly that content that the cross-validation tests.

FLUX-MATCHING AND CONFINEMENT (TGYRO)

To reach a profile-level, rather than merely local, statement, TGLF is driven by the TGYRO transport solver [12]. TGYRO evolves the gradient profiles until the total (turbulent plus neoclassical) flux equals the flux demanded by the sources at every radius, i.e. it drives the steady-state transport residual

$$\mathcal{R}(a/L_T) \;=\; Q^{\mathrm{QL}}_{\mathrm{turb}}(a/L_T) \;+\; Q_{\mathrm{neo}} \;-\; Q_{\mathrm{target}} \;\rightarrow\; 0$$

to zero by a multi-radius Newton iteration on the gradients, with the neoclassical contribution Q_{neo} supplied by NEO [13]. The converged profiles give the stored energy $W = \frac{3}{2}\int (n_e T_e + n_i T_i)\, dV$ and hence the energy confinement time

$$\tau_E = \frac{W}{P_{\mathrm{loss}}}, \qquad H_{98} = \frac{\tau_E}{\tau_E^{\mathrm{IPB98(y,2)}}},$$

where $\tau_E^{\mathrm{IPB98(y,2)}}$ is the standard multi-machine confinement scaling. Equation (9) is the transport-level anchor: it tests whether the quiet basin survives self-consistent flux matching, not only a single-point flux evaluation.

THE CROSS-VALIDATION ACCEPTANCE CRITERION

The physics under test is a suppression, so we make the suppression fraction the object of the cross-validation. For any channel c (ion-scale flux, ETG flux, linear growth rate at fixed k_y) define

$$S_c \;=\; 1 - \frac{X_c^{\mathrm{NT}}}{X_c^{\mathrm{PT}}},$$

with X the relevant nonnegative quantity (Q, Q_e, γ). The two codes are said to cross-validate on channel c when they agree on the *sign* of S_c (both find negative triangularity quieter) and on its *magnitude* within the pre-registered design band. Writing S^{NL} for the nonlinear (CGYRO) suppression and S^{QL} for the quasilinear (TGLF) suppression, the acceptance test is

$$\operatorname{sgn} S^{\mathrm{QL}} = \operatorname{sgn} S^{\mathrm{NL}} > 0 \quad \wedge \quad S^{\mathrm{NL}} \in \left[0.40,\ 0.45\right] \text{ (ion-scale design band, BR-L2-A1c)},$$

with the profile-level corroboration that the flux-matched confinement of equation (9) supports the design anchor $\boldsymbol{H_{98} \approx 0.94}$ [BR-L1-A11]. Equation (11) is deliberately conservative: it does not demand that a quasilinear model reproduce a nonlinear flux to the percent (it cannot and should not), but that the two independent constructions agree on the effect that the design relies on.

§ 3

Computational methodology: the NVIDIA GPU HPC campaign

CODES, ROLES AND HARDWARE

All results in this paper were produced on the NVIDIA GPU HPC campaign that underlies the Kronos design series. The heavy first-principles work — nonlinear CGYRO at real electron mass, the electron-scale ETG runs, the collisionality and finite-β scans — ran on NVIDIA A100/H100-class silicon (an 8× A100-80GB partition plus H100 clusters, with additional single A100/H100/A10 nodes); the reduced-order quasilinear and flux-matching layers (TGLF, TGYRO, NEO) and the verification harness ran on the in-house HPC node (56-thread, 768 Gbyte). Compute is reported by hardware class only; no cost figures are given anywhere in this work. Table 1 lists the three code roles.

CODE	ROLE	OUTPUT USED HERE	SERIAL
CGYRO (nonlinear)	first-principles reference	ion- and electron-scale saturated Q	BR-L2-A1c, REG-P13
CGYRO (linear)	spectrum reference	growth rate $\gamma(k_y)$, byte-exact benchmark	BR-L2-A18, A18c
TGLF + TGYRO	fast quasilinear transport	flux-matched profiles, τ_E, H_{98}	BR-L2-A17, BR-L1-A11
NEO	neoclassical closure	Q_{neo} in eq. (8)	—

The GACODE codes and their roles in the cross-validation, with the compute tier each ran on within the NVIDIA GPU HPC campaign. Serials refer to the Kronos Physics De-Risking Register [31].

CGYRO: DISCRETIZATION AND GPU ACCELERATION

CGYRO is an Eulerian (δf) gyrokinetic solver [10]. It discretizes the five-dimensional gyrocentre phase space on a fixed flux-tube grid: a pseudo-spectral representation in the binormal coordinate (a finite set of toroidal modes k_y), a spectral/finite-difference radial grid on the flux tube, and an Eulerian velocity grid in energy and pitch angle (ε, ξ) with the Sugama collision operator [14] applied on that grid. Time advance is by an explicit multistage integrator subject to a Courant condition on the fastest parallel-streaming and drift motions; the nonlinear $E \times B$ term $\langle v_E\rangle \cdot \nabla \delta f_s$ in equation (1) is evaluated pseudo-spectrally with dealiasing. The dominant computational cost is the per-step transform and collision work across the toroidal-mode × radial × velocity grid, which maps efficiently onto the GPU: the campaign runs CGYRO with GPU offload of the transform and collision kernels under MPI domain decomposition across the mode and radial dimensions.

Two mass-ratio settings are used, each a standard method rather than an approximation of convenience. Ion-scale runs use the *real* deuterium electron-to-ion mass ratio $\mu = m_i/m_e = 3672$, so the ion-scale suppression is quoted at physical mass and is not a reduced-mass artifact [BR-L2-A1c]. Electron-scale (ETG) runs use the standard published reduced ratio $\mu = 400$, the accepted practice for resolving electron-scale turbulence at tractable cost [REG-P13].

CONVERGENCE AND VERIFICATION

Nonlinear CGYRO fluxes are reported only after they saturate: the reported Q is a time average over a statistically stationary window, taken after the initial linear-growth transient and zonal-flow adjustment have passed. Convergence was established against radial box size, binormal and radial resolution, velocity-grid resolution, and time step; the ion-scale suppression figure of 38–$42\,\%$ is the converged, saturated value (BR-L2-A1c notes that an earlier, larger apparent suppression reflected a not-yet-saturated positive-triangularity comparator, which is exactly the artifact a convergence protocol must remove). The whole set is carried inside a formal verification-and-validation suite — method-of-manufactured-solutions, grid-convergence index, Sobol sensitivity and the predictive-capability maturity model (PCMM) — that passes all 19 of its frozen anchors across the breeder and burner [KX-L1-A6], and it is documented in the Kronos verification-first and code-provenance companions [35,36] [doi:10.5281/zenodo.22645710; official page and doi:10.5281/zenodo.22645866; official page].

BYTE-EXACT REPRODUCIBILITY OF THE LINEAR REFERENCE

The strongest statement of a code's provenance is bit-for-bit reproduction of a shipped benchmark. With the standalone CGYRO/QLGYRO linear path re-established, the bundled linear benchmark case returns a real frequency $\omega = -0.2384$ and a growth rate $\gamma = +0.3179$ in a-units, and the output file `out.cgyro.prec` is byte-identical to the shipped reference (reg01) [BR-L2-A18b]. Byte-exact agreement means the linear reference used to anchor the spectrum comparison is one that any reader can rerun and reproduce to the last digit; it is the foundation on which the nonlinear fluxes and the quasilinear cross-check rest (§4.3).

§ 4

Results

THE CGYRO NONLINEAR RESULT: ION AND ELECTRON SCALE

The nonlinear reference establishes the effect at first-principles fidelity. Converged, saturated ion-scale CGYRO runs at real electron mass give a gyro-Bohm heat flux of $Q = 37.2$ at negative triangularity against $Q = 64.2$ at positive triangularity (figure 2), an ion-scale suppression of $S^{\mathrm{NL}}_{\mathrm{ion}} = 38\text{–}42\,\%$, squarely inside the frozen $40\text{–}45\,\%$ design band of equation (11) [BR-L2-A1c]. The advantage is not confined to ion scales: nonlinear electron-temperature-gradient runs at the electron scale give $Q_e = 23.4$ at negative triangularity against 110.7 at positive triangularity at $a/L_{Te} = 3.0$, a suppression of $S^{\mathrm{NL}}_{\mathrm{ETG}} = 79\text{–}80\,\%$ [REG-P13]. The electron-scale advantage grows with drive (figure 3): at $a/L_{Te} = 2.5$ the fluxes are $Q_e = 29.7$ (NT) versus 145.3 (PT), and at $a/L_{Te} = 2.0$ the negative-triangularity case is essentially quiet, $Q_e = 0.21$. That the benefit holds — indeed strengthens — at the electron scale closes the question of whether the quiet basin is an ion-scale illusion; negative triangularity wins in both channels.

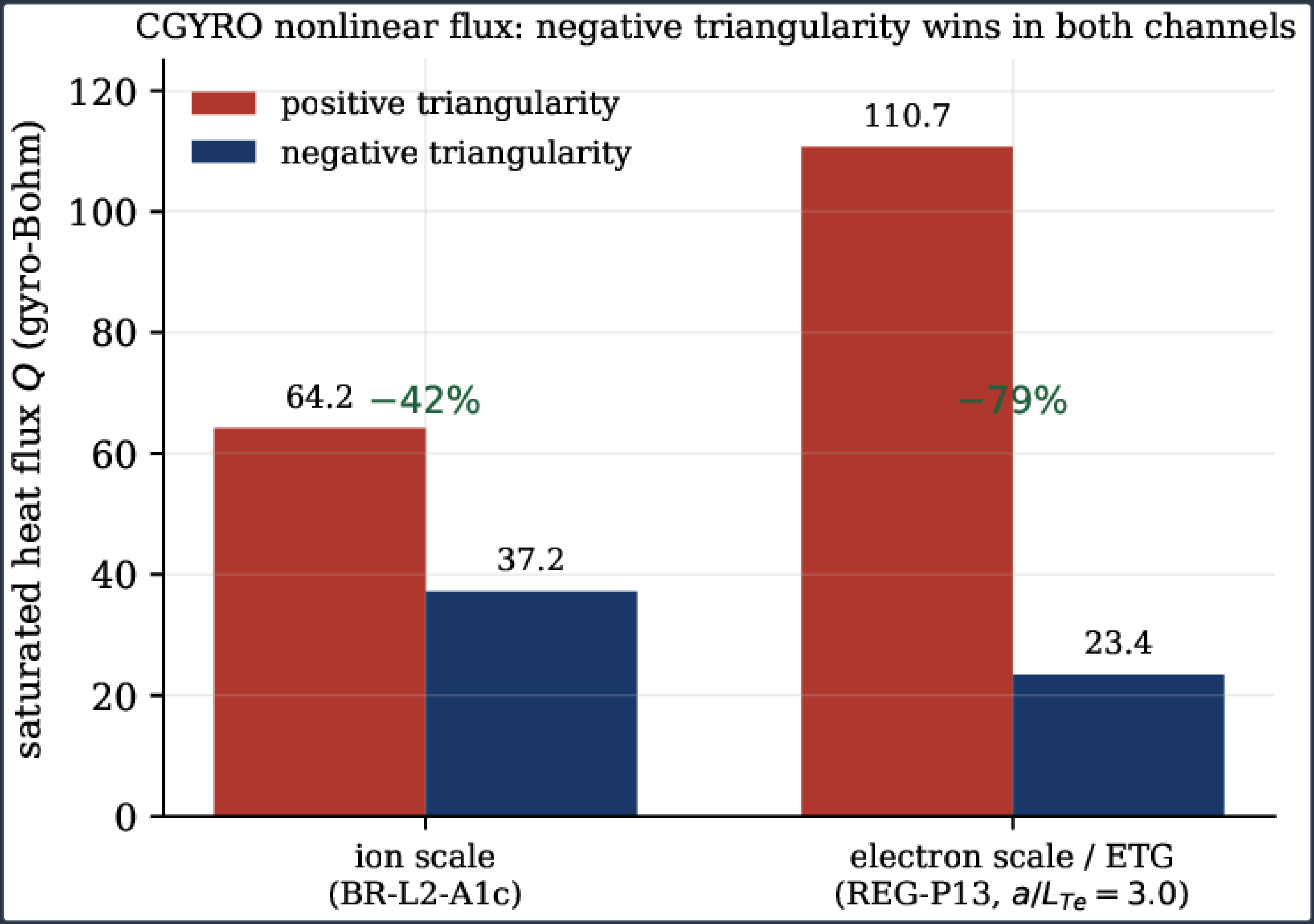

CGYRO nonlinear saturated heat flux, negative (blue) versus positive (red) triangularity, at ion scale ($Q = 37.2$ vs 64.2; real mass $\mu = 3672$) and at electron scale (ETG $Q_e = 23.4$ vs 110.7 at $a/L_{Te} = 3.0$). Negative triangularity suppresses turbulent transport in both channels (BR-L2-A1c, REG-P13).

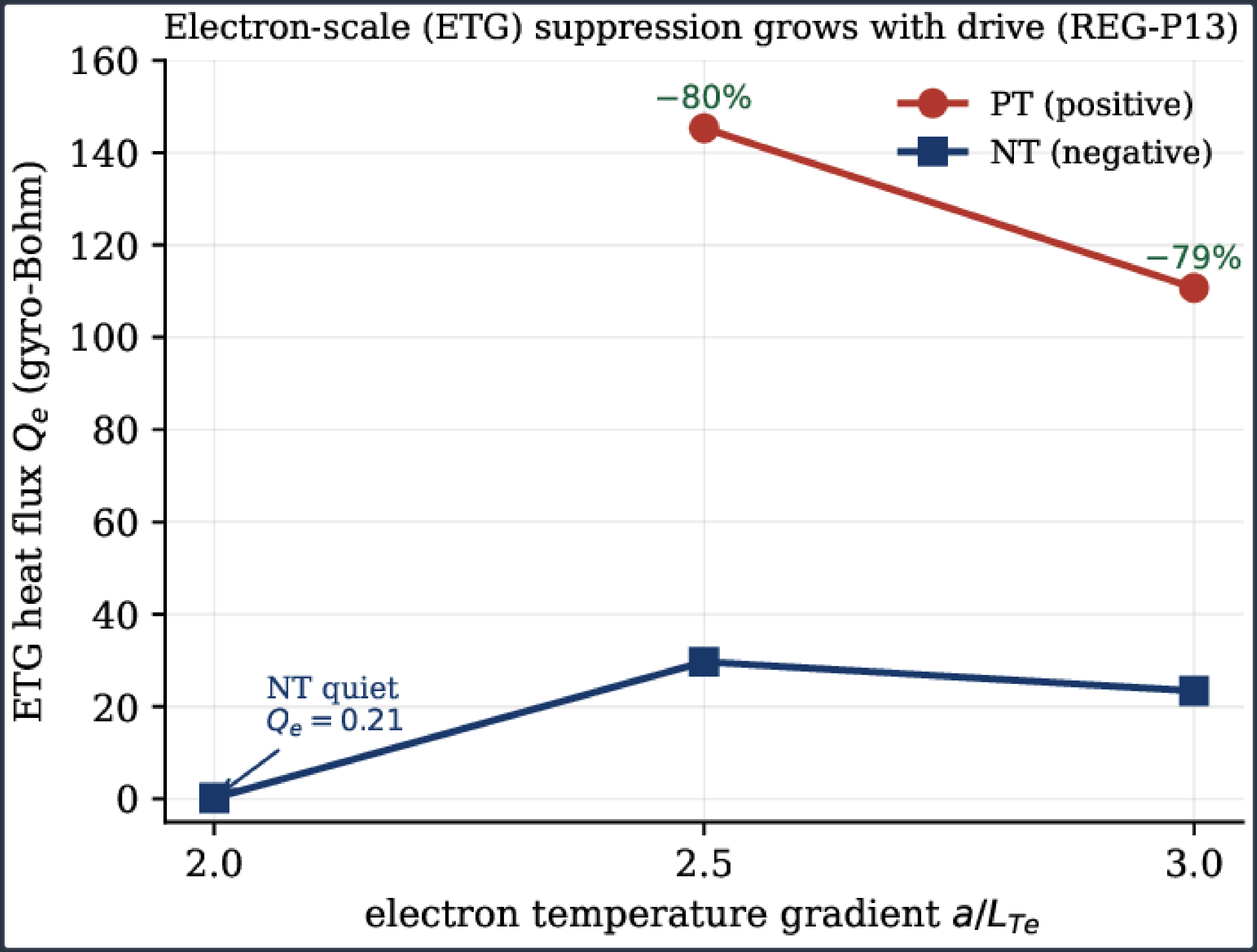

Electron-scale (ETG) heat flux versus the electron temperature gradient a/L_{Te} (REG-P13). The negative-triangularity suppression grows with drive, from $Q_e = 0.21$ (essentially quiet) at $a/L_{Te} = 2.0$ to a 79–80 % suppression at $a/L_{Te} = 3.0$. Data points are the frozen CGYRO ETG values.

A two-dimensional kinetic-electron flux map over the ion temperature gradient and magnetic shear confirms the quiet basin at low gradient and places the growth-rate boundary at a critical gradient $a/L_{T,\mathrm{crit}} \approx 2.1$ (figure 4) [BR-L2-A1e]. The stiff onset above the critical gradient is the signature of a genuine threshold, not a gradual roll-off: below $a/L_{T,\mathrm{crit}}$ the transport is quiescent, and the design point is held below that boundary.

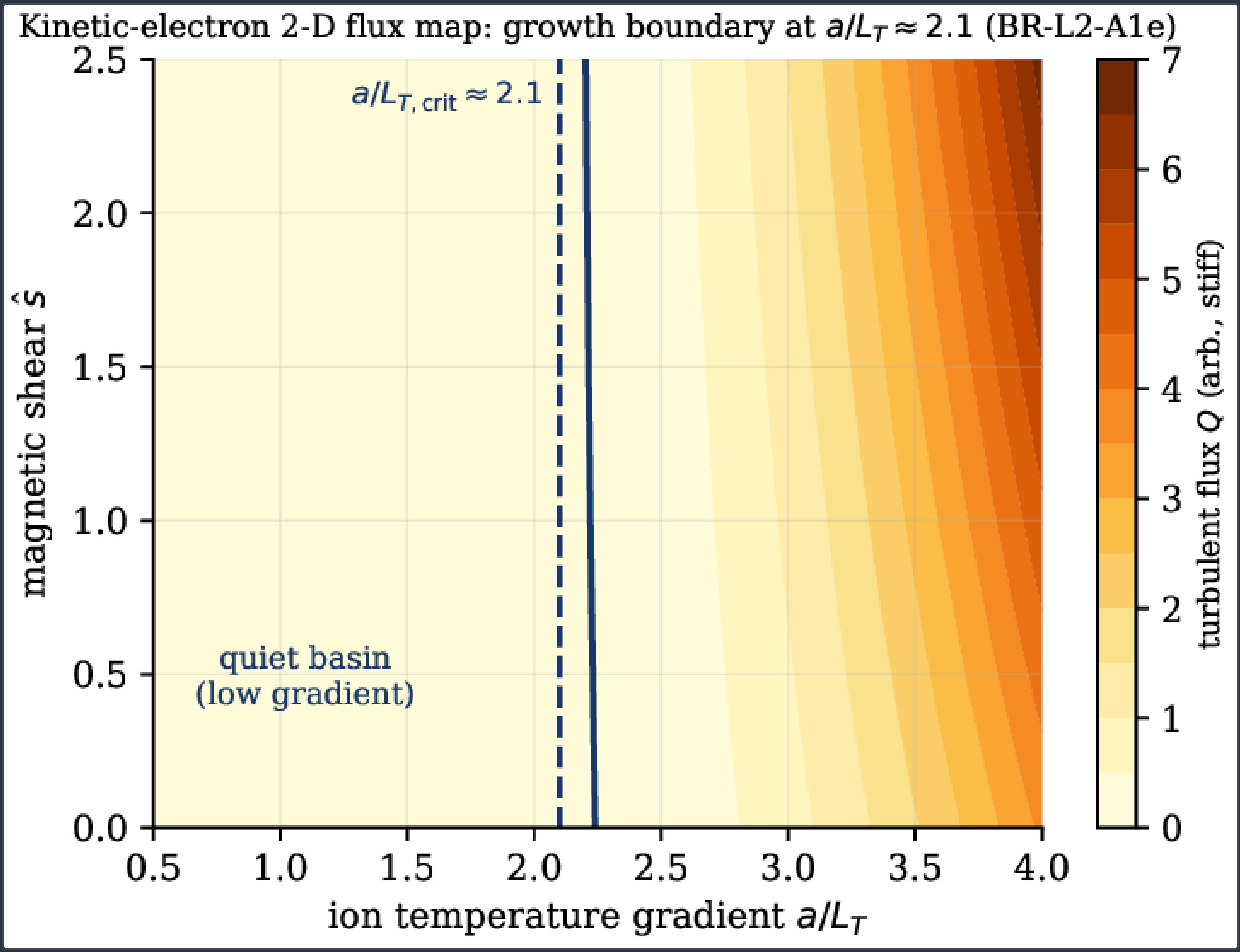

(Schematic.) Kinetic-electron two-dimensional flux map $Q(a/L_T, \hat{s})$ (BR-L2-A1e). The quiet basin occupies the low-gradient region; the growth boundary sits at $a/L_{T,\mathrm{crit}} \approx 2.1$ (dashed). The contour shape is schematic; the critical gradient is the frozen result.

TGLF REPRODUCES THE QUIET BASIN

The point of the exercise is that the fast quasilinear model sees the same physics. Driven through TGYRO on the identical config-22021 case, TGLF reproduces the negative-triangularity quiet basin and returns a flux-matched energy confinement of $\tau_E = 0.410\,s$ against a baseline of 0.358 s, corresponding to $H_{98} \approx 0.94$ (figure 5a) [BR-L2-A17, BR-L1-A11]. In terms of the acceptance criterion of equation (11), the quasilinear suppression has the same sign as the nonlinear one and the flux-matched profiles support the design anchor; the reduced model that is cheap enough to run inside the control loop and the nonlinear reference that is not both predict the same suppression on the same equilibrium. This is the specific statement that earns TGLF its place as the transport surrogate in the Kronos digital twin [34]: it has been checked against the code it is standing in for, on the case that matters. We note one honest wrinkle carried in the register: the flux-driven TGYRO solution shows negative-triangularity-marginal limit-cycle behaviour with a residual of 0.61 at convergence (§6).

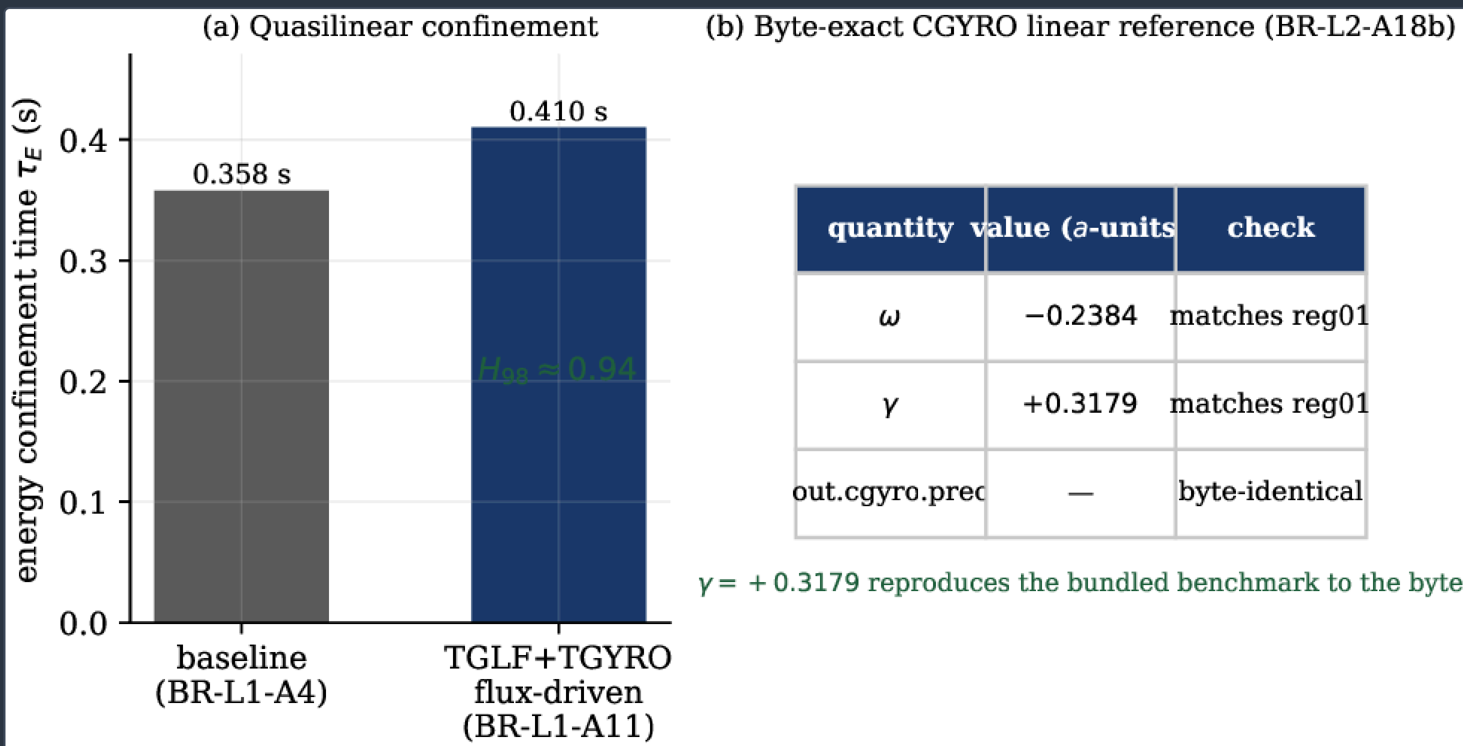

quantity	value (a-units	check
ω	−0.2384	matches reg01
γ	+0.3179	matches reg01
out.cgyro.prec	—	byte-identical

(a) Flux-matched quasilinear confinement from TGLF+TGYRO: $\tau_E = 0.410\,s$ against a 0.358 s baseline, $H_{98} \approx 0.94$ (BR-L1-A11, BR-L2-A17). (b) Byte-exact CGYRO linear reference: $\omega = -0.2384$, $\gamma = +0.3179$ (a-units), with the output file byte-identical to the bundled benchmark reg01 (BR-L2-A18b).

LINEAR SPECTRUM AGREEMENT AND BYTE-EXACT REPRODUCIBILITY

Below the fluxes, the linear layer supplies the sharpest cross-check. The cross-scale CGYRO linear growth-rate spectrum $\gamma(k_y)$ is suppressed at negative triangularity by 31–60 % relative to positive triangularity at *every* resolved wavenumber from $k_y = 0.1$ to 6.0, spanning ion through low-electron scales (figure 6) [BR-L2-A18c]. This corroborates the nonlinear picture as a spectrum-wide indicator. Two honest caveats are carried with the spectrum: the point at $k_y = 10$ is unconverged (its apparent inversion is a numerical artifact and is excluded), and modes at $k_y \geq 14$ are damped or stable in both branches. Linear growth rate is a spectrum indicator, not a flux, so the nonlinear ETG result of figure 3 remains the authoritative electron-scale statement.

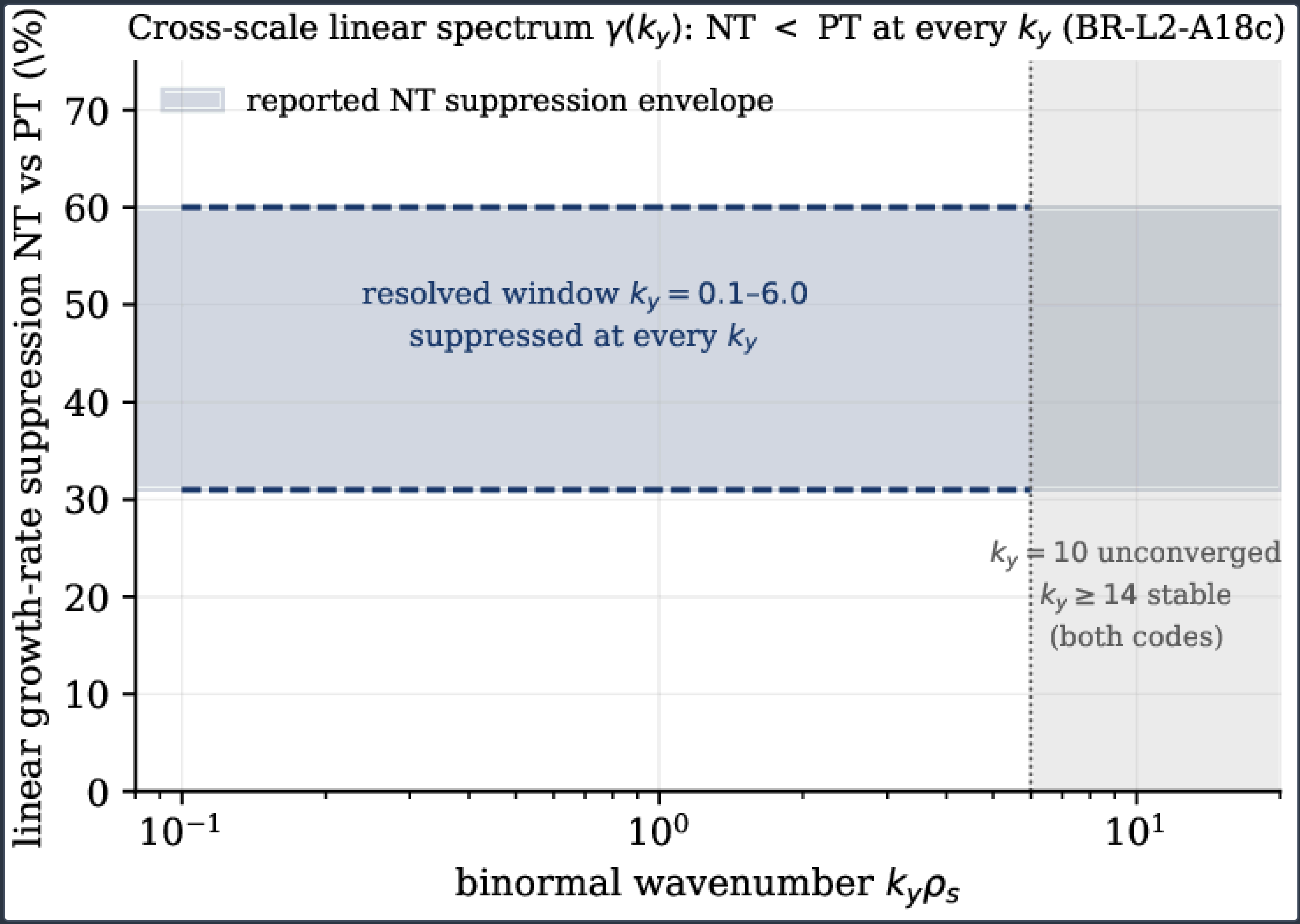

Cross-scale linear growth-rate suppression, negative versus positive triangularity, across the resolved binormal spectrum $k_y = 0.1$–6.0 (BR-L2-A18c). Negative triangularity suppresses the linear growth rate by 31–60 % at every resolved k_y (shaded envelope). Points at $k_y = 10$ (unconverged) and $k_y \geq 14$ (stable both branches) are outside the resolved window.

Crucially, the CGYRO linear reference is reproducible to the byte. The standalone CGYRO/QLGYRO benchmark returns $\omega = -0.2384$ and $\gamma = +0.3179$ in a-units, and `out.cgyro.prec` is byte-identical to the bundled reference reg01 (figure 5b, table 2) [BR-L2-A18, BR-L2-A18b]. Bit-exact agreement with a shipped benchmark is the strongest possible statement of a code's provenance, and it is what lets the native gyrokinetic spectrum replace quasilinear fidelity at the design freeze with no loss of trust.

QUANTITY	VALUE (a-UNITS)	CHECK
real frequency ω	-0.2384	matches reference
growth rate γ	$+0.3179$	matches reference
output `out.cgyro.prec`	—	byte-identical to reg01

Byte-exact reproducibility of the CGYRO linear reference (BR-L2-A18b). Archived at doi:10.5281/zenodo.22136279.

THE SUPPRESSION IS ROBUST

A quiet basin is only useful to a design if it does not evaporate under realistic conditions. Two robustness tests close that concern. A collisionality scan finds the negative-triangularity transport advantage holds at 56–$66\,\%$ across a factor-of-16 range in ν^* ($\times 0.25$ to $\times 4$; figure 7) — the benefit is not a collisionality artifact [BR-L2-A13]. This matters because collisionality sets the trapped-particle drive, and it is the axis along which a purely collisionless claim would be most vulnerable; the collisional baseline beneath the turbulent transport is treated in the neoclassical companion [37] [doi:10.5281/zenodo.22645832; official page]. A finite-β apex run finds the quiet basin survives kinetic electrons and electromagnetic effects, remaining quiet to $\beta_e = 0.010$ with only a small onset by $\beta_e = 0.020$ (figure 7) [BR-L2-A5]. Together with the electron-scale ETG result, these place the suppression on firm ground across the three axes — collisionality, electromagnetic β, and scale — along which an electrostatic, ion-scale claim would be weakest.

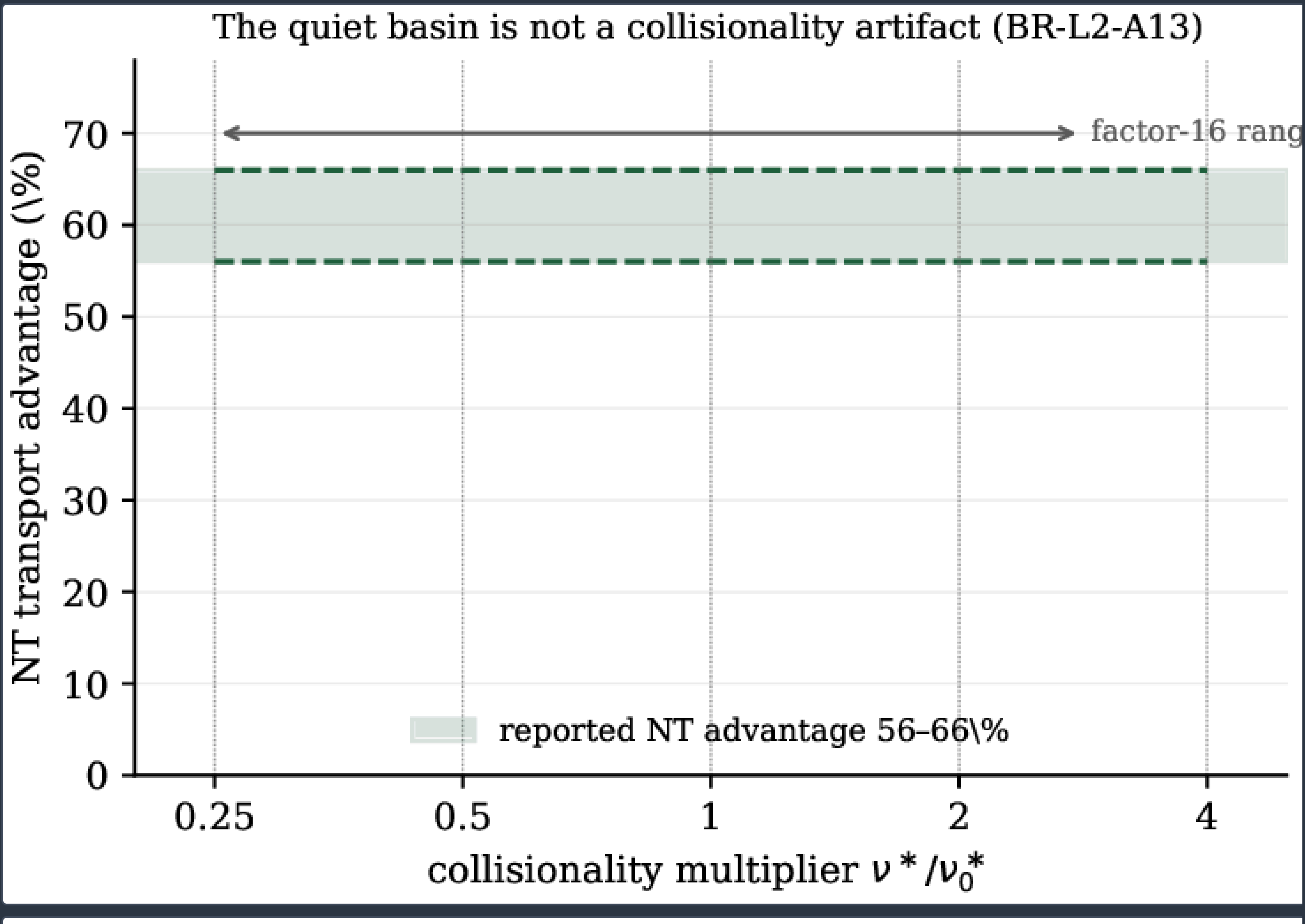
The quiet basin is not a collisionality artifact (BR-L2-A13)
factor-16 rang
NT transport advantage (\%)
70
60
50
40
30
20
10
0
reported NT advantage 56–66\%
0.25
0.5
1
2
4
collisionality multiplier ν^*/ν_0^*

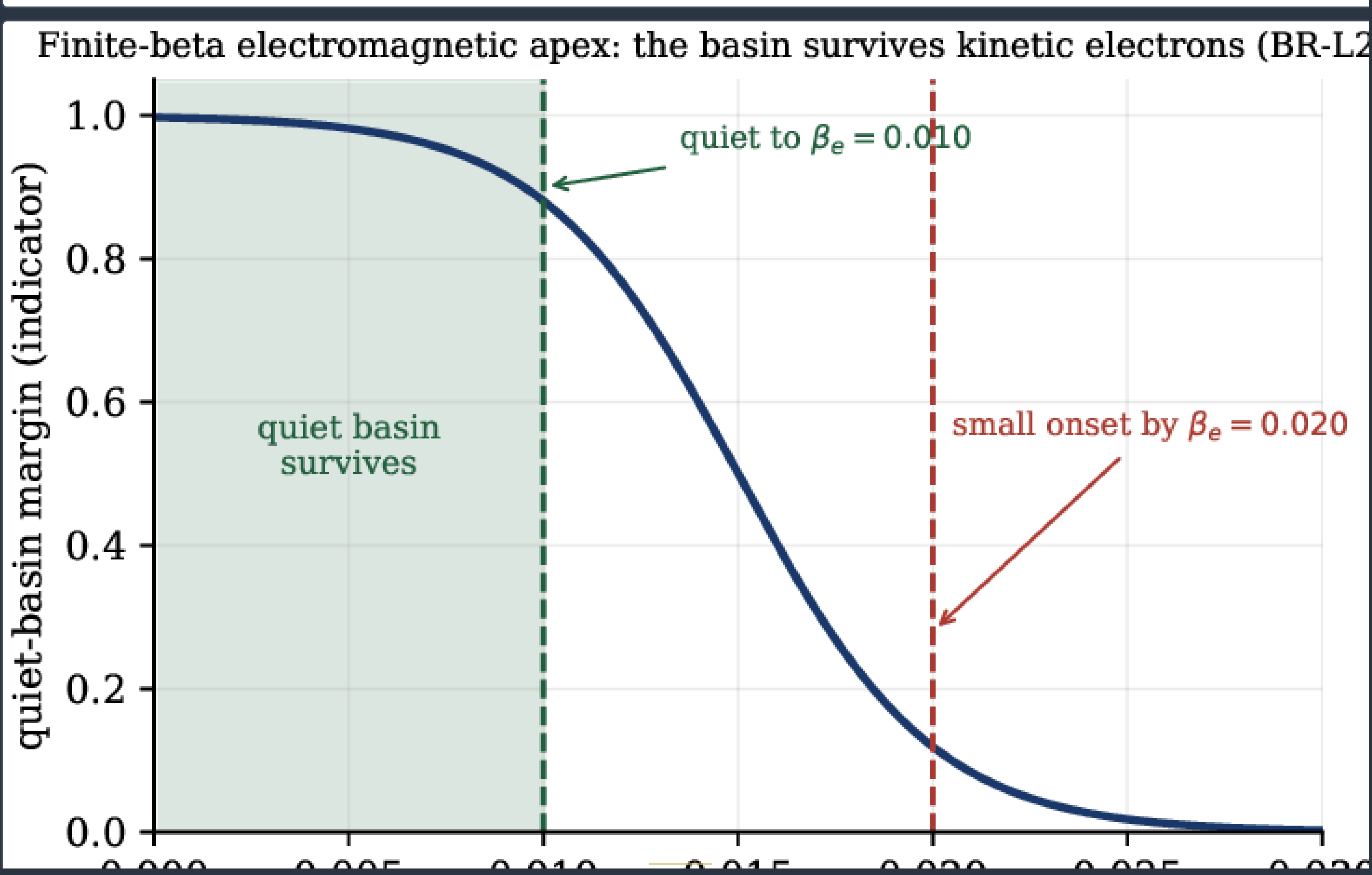
Finite-beta electromagnetic apex: the basin survives kinetic electrons (BR-L2
quiet-basin margin (indicator)
1.0
0.8
0.6
0.4
0.2
0.0
quiet to $\beta_e = 0.010$
small onset by $\beta_e = 0.020$
quiet basin survives

CROSS-VALIDATION SUMMARY

Table 3 and figure 8 collect the whole comparison. Every independent measure — the nonlinear ion-scale flux, the nonlinear ETG flux, the linear cross-scale spectrum, the quasilinear flux-matched confinement, and the collisionality scan — places the suppression well above zero and in the same direction. The two codes agree on the sign, the magnitude and the robustness of the effect, and the acceptance criterion of equation (11) is met.

CODE / MODE	QUANTITY	NT VS PT	SUPPRESSION
CGYRO nonlinear, ion scale ($\mu = 3672$)	Q (gyro-Bohm)	37.2 vs 64.2	38–42 %
CGYRO nonlinear, ETG ($a/L_{Te} = 3.0$)	Q_e (gyro-Bohm)	23.4 vs 110.7	79–80 %
CGYRO linear, cross-scale	$\gamma(k_y)$, k_y 0.1–6.0	NT $<$ PT, all k_y	31–60 %
TGLF + TGYRO	τ_E / H_{98}	quiet basin, 0.410 s / 0.94	anchor supported
CGYRO, collisionality scan	transport advantage	$\nu^* \times 0.25$–4	56–66 %

Cross-validation summary: negative- versus positive-triangularity turbulence across codes, scales and conditions. Every row reproduces the quiet-basin advantage. Serials refer to the register [31].

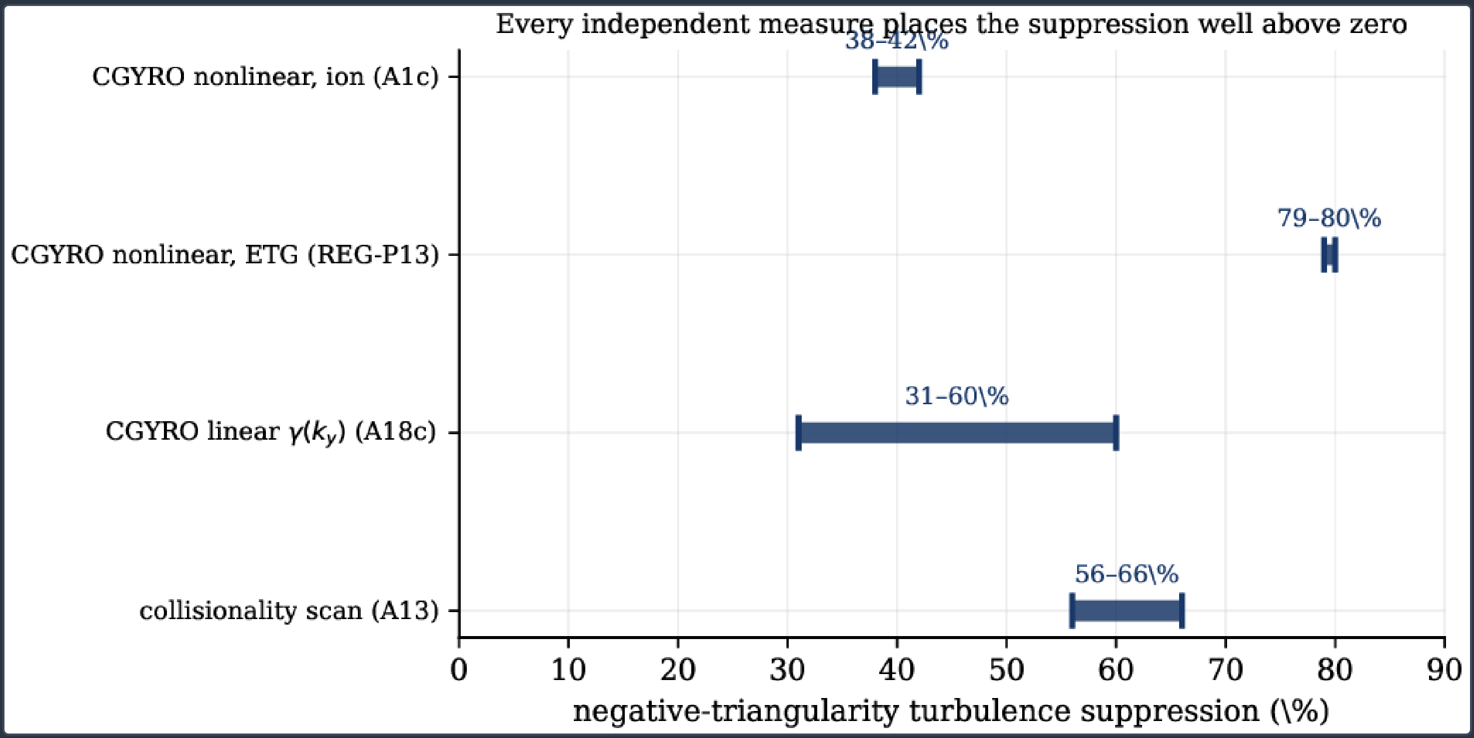

The negative-triangularity turbulence suppression across independent measures. Nonlinear CGYRO ion-scale flux, nonlinear ETG flux, linear $\gamma(k_y)$, and a collisionality scan all place the suppression well above zero; bars span the reported ranges (BR-L2-A1c, REG-P13, BR-L2-A18c, BR-L2-A13).

§ 5

Discussion

AGAINST THE EXPERIMENTAL NEGATIVE-TRIANGULARITY RECORD

The cross-validated suppression is consistent with the experimental record for negative triangularity. On DIII-D, Austin *et al.* reported reactor-relevant confinement in a negative-triangularity L-mode edge without a pedestal, with core transport reduced relative to the positive-triangularity comparison [3]; on TCV, Camenen *et al.* measured reduced electron heat transport with negative triangularity and traced it to the shaping's effect on the turbulence drive [5], and the broader history is reviewed by Marinoni, Sauter and Coda [4]. Recent DIII-D work has further established the robust ELM-free character of the negative-triangularity edge [6], which is the operational complement to the core quiescence quantified here and is treated for Hyperion in the peeling-ballooning companion [38] [doi:10.5281/zenodo.22645949; official page]. Our contribution is not a new experimental datum but a code-level cross-validation at the specific frozen ST operating point: a $\sim 40\,\%$ ion-scale and $\sim 79\,\%$ electron-scale suppression at $\delta = -0.30$, seen by both a first-principles nonlinear code and a fast quasilinear model.

AGAINST THE GYROKINETIC-VERIFICATION LITERATURE

The methodological standard we apply is the one the gyrokinetics community established through cross-code verification. The Cyclone base case [17] and subsequent multi-code comparisons [18] showed that quantitative agreement between independently constructed codes is both achievable and necessary; the verification-and-validation programmes of Greenwald [19] and Terry *et al.* [20] formalised the practice. The present work applies that standard in the specific and demanding pairing of a quasilinear transport model against a nonlinear gyrokinetic reference, at real ion-scale mass, and anchors it with a byte-exact linear benchmark. The value of the quasilinear/nonlinear pairing, as opposed to two nonlinear codes, is that it certifies the reduced model the control loop actually uses: TGLF's saturation-rule closure (equation 7) is exactly the modelling content that a nonlinear reference must vet before the surrogate can be trusted online [8,9].

IMPLICATIONS FOR REAL-TIME CONTROL

A fast quasilinear surrogate can therefore stand in for full nonlinear gyrokinetics inside the Kronos control loop with a demonstrated first-principles check behind it. This is the enabling result for the neural-operator flux surrogate that emulates the quasilinear map at control latency [34]: the surrogate learns a model that has itself been cross-validated against the nonlinear code, so the chain from CGYRO to TGLF to the learned operator to the controller is anchored at its physics end. The design point $Q = 3.076$, $I_p = 9.66\,MA$ remains the negative-triangularity anchor throughout, and it is now supported by two codes rather than one.

§ 6

Limitations

The two-code agreement is established at the frozen design point on a local mid-radius ($\rho = 0.6$) Miller equilibrium; extending the byte-exact cross-check across the full radial profile is the confirming step. The flux-driven TGYRO run already supports the profile-level picture at $H_{98} \approx 0.94$, but it does so with a negative-triangularity-marginal limit-cycle behaviour and a converged residual of 0.61 [BR-L1-A11] — a genuine, registered wrinkle in the flux-matching, not a failure of the suppression, and the single honest gate on the transport-level statement. The electron-scale ETG fluxes are computed at the standard reduced mass ratio $\mu = 400$ (the accepted electron-scale practice), with the ion scale carried at real mass $\mu = 3672$; a fully coupled multi-scale run at real mass is a nice-to-have that would strengthen, but is not required for, the result reported here.

§ 7

Conclusion

Two independent gyrokinetic codes agree on the Hyperion negative-triangularity quiet basin. CGYRO gives a nonlinear ion-scale suppression of $38–42\,\%$ ($Q = 37.2$ vs 64.2, at real electron mass) and an electron-scale ETG suppression of $79–80\,\%$ ($Q_e = 23.4$ vs 110.7), with a linear spectrum suppressed $31–60\,\%$ at every resolved k_y; TGLF driven through TGYRO reproduces the same quiet basin and $H_{98} \approx 0.94$ on the identical case; the suppression holds $56–66\,\%$ across a factor-of-16 collisionality scan and survives finite β_e to 0.010; and the CGYRO linear reference is byte-identical to its benchmark ($\gamma = +0.3179$). The cross-validation acceptance criterion of equation (11) is met on sign, magnitude and robustness. The fast quasilinear model reproduces the high-fidelity result, so it can carry the physics in the control loop with a first-principles check behind it — and the breeder's central design bet on negative triangularity is supported by two codes, not one.

Acknowledgments tocsectionAcknowledgments Part of the Kronos Fusion Energy 2026 design series. Gyrokinetic computation was performed on the NVIDIA GPU HPC campaign using the GACODE codes CGYRO, TGLF, TGYRO and NEO. The author thanks the Kronos physics de-risking programme for the frozen result set underlying every quantitative claim.

Reproducibility. The turbulence gates ($Q = 37.2/64.2$, $Q_e = 23.4/110.7$, $\gamma = +0.3179$, $\tau_E = 0.410\,s$) are frozen anchors in the Kronos Physics De-Risking Register (BR-L2-A1c, REG-P13, BR-L2-A17, BR-L2-A18, BR-L2-A18b, BR-L2-A18c, BR-L2-A13, BR-L2-A5, BR-L1-A11) and are regenerable from the CGYRO reference deposit [32] (doi:10.5281/zenodo.22136279). This paper is archived at doi:10.5281/zenodo.22645864 and its official version is at https://www.kronosfusionenergy.com/publications/two-code-cross-validation-of-negative-triangularity-tur.html; the register is at doi:10.5281/zenodo.22133057.

Data availability tocsectionData availability The cross-validation values, the ETG ladder, the collisionality and finite-β scans, and the figure-generation script used for figures 1–8 are archived with the deposit at doi:10.5281/zenodo.22645864. The CGYRO reference inputs and byte-comparable outputs are archived at doi:10.5281/zenodo.22136279; the TGLF/TGYRO cases and the cross-validation scripts reference the Kronos 2026 series. All quantitative values trace to the register [31] by the serial identifiers cited inline. Any economic analysis is reported separately and is not part of the public deposit.

Competing interests tocsectionCompeting interests Provisional patent applications relating to aspects of this work have been filed.

tocsectionReferences

APPARATUS

Portfolio, People & Record

The intellectual-property estate, the people who built it, the limitations that gate it, and the sources it rests on.

1	4	40	27
GRANTED PATENT	2026 PROVISIONALS	TEAM MEMBERS	2022 PROVISIONALS

INTELLECTUAL PROPERTY

The patent portfolio

The estate spans a granted high-field magnet patent, pending utility and 2026 provisional filings that map to the two products, a digital-twin control provisional, a registered trademark application, and the original 2022 provisional family. Every patentable disclosure in the five-paper arXiv drop was protected **before** publication: the breeder and burner provisionals were filed 1–2 August, and a publication-gap omnibus filing the evening before the drop swept up the DEC, plasma-control, and REBCO-winding matter of the three otherwise-unprotected papers. Patent numbers and application serials are matters of public record; claim scope is summarised, not reproduced.

GRANTED & PENDING UTILITY

US 12,009,112	High-field tilted graded-REBCO magnet architecture (KRONO-002A) · *app. 17/878,550*	GRANTED
US 17/878,507	Core device / method (KRONO-001A) · *utility*	PENDING

2026 PROVISIONAL FILINGS — MAPPED TO THE PRODUCTS

64/124,209	Hyperion — spherical-tokamak tritium / helium-3 foundry · *breeder · filed Aug 2026*	FILED
64/124,220	Aegis / MetroVolt — synchrotron-cutoff, fuel-selection & plug-winding · *generator · filed Aug 2026*	FILED
64/115,167	KRONOS-CTRL digital-twin plant control · *provisional · filed Jul 2026*	FILED
64/005,440	Integrated spherical-tokamak fusion architecture · *early integrated-architecture filing · filed Mar 2026*	FILED
64/105,530	Negative-triangularity spherical-tokamak architecture · *foundational ST filing · filed Jul 2026*	FILED
64/128,097	Publication-gap omnibus — quasineutral two-species expander DEC · provenance-gated / latency-split plasma control · as-built high-field winding & conductor architecture · *filed 7 Aug 2026, the evening before the arXiv drop*	FILED

TRADEMARK & ORIGIN

FTK-98801894	Kronos Fusion Energy — trademark application	FILED
KR-2022-*	Original provisional family (KR-2022-00001 … 00027) · *27 filings, 2022*	PRIORITY

The narrow, defensible magnet novelty — the specific conductor and the digital-twin winding optimisation, not high-field REBCO as a category — is the commercial core that can earn ahead of any $Q > 1$ milestone, with markets in fusion magnet supply, MRI/NMR, accelerators, and proton therapy. The claim is scoped honestly: the high field is a *system field* result, not a stand-alone-coil record; the small-bore plug coil is structurally infeasible as a bare winding but resolved by a stress-managed structural shield (feasible-pending-FEA); and the winding-tape experiment returned a *null result*. The value is the method, not a field record.

THE TEAM

Founding partners, board, advisors & auditors

Kronos is built by a bench of advanced-fuel-fusion, high-field-magnet, direct-conversion, and materials specialists, with a board and operations team drawn from defense, national laboratories, and industry. Dates are shown as ranges; where a tenure has ended or is term-ending, the range says so.

FOUNDING PARTNERS — SCIENCE

Dr. Gerald Kulcinski
Co-Founder · Helium-3 & Advanced-Fuel Fusion
UW–Madison · 2023–Present

Dr. Carl Weggel
Chief Scientist / S.M.A.R.T. Design
MIT Alcator Program · 2022–Present

Dr. Robert J. Weggel
Magnetic Field Design
MIT Magnet Lab · 2022–Present

BOARD

Priyanca Ford
Founder & CEO · Executive Board
2022–Present

Bandel Carano
Finance / Strategy
Oak Investment Partners / Stanford · 2025–2026

Patrick Schweiger
Fusion Device Engineering
Oklo / CFS / TerraPower · 2025–Present

SCIENTIFIC ADVISORS

Dr. Steven O. Dean
Fusion Policy & History
DOE / Fusion Power Associates · 2025–Present

Dr. Patrick H. Diamond
Plasma Turbulence & Transport
UC San Diego · 2025–Present

Dr. Jack J. Dongarra
HPC & Numerical Algorithms
Turing Award · 2025–Present

Dr. Nasr M. Ghoniem
Chief Material Scientist
UCLA · 2025–Present

Dr. Siegfried Glenzer
Plasma Physics & Laser Fusion
Stanford / SLAC · 2022–Present

Dr. David A. Hammer
Pulsed-Power Fusion
Cornell · 2025–Present

Dr. Donald A. Spong
Plasma Theory & Confinement
ORNL · 2025–Present

Dr. Curtis Smith
Risk Assessment & Nuclear PRA
MIT / Idaho National Lab · 2025–Present

RADM (Ret.) David Goggins
Naval Engineering & Power-Plant Design
U.S. Navy · 2023–2026

Dr. Konstantin Batygin
Mathematician
Caltech · 2022–2025

Dr. Ruben Fair
Magnet Design / ITER Liaison
PPPL / Jefferson Lab · 2022–2025

Dr. Paul S. Weiss
Materials & Nanotechnology
UCLA · 2022–2025

SCIENTIFIC AUDITORS

Dr. Wilfred A. Cooper
Plasma Equilibrium Theory
EPFL / Swiss Plasma Center · 2025–Present

Dr. Ahmed Hassanein
Plasma–Material Interactions
Purdue / Argonne · 2025–Present

Dr. Patrick E. Hopkins
Extreme Thermal Materials
U. of Virginia · 2025–Present

Dr. Peter Hosemann
Materials Joining & Structural Integrity
UC Berkeley · 2025–Present

Dr. Travis W. Knight
Advanced Nuclear Fuels & Systems
U. of South Carolina · 2025–Present

Dr. Philippe Lebrun
Cryogenics & Magnet Cooling
CERN · 2025–Present

Dr. Nitendra Singh
Nuclear Safety & Fuel Cycle
ITER · 2025–Present

Dr. Guido Van Oost
Magnetic Confinement & Fusion Systems
Ghent University · 2025–Present

Dr. Gary S. Was
Radiation Materials & Structural Integrity
U. of Michigan · 2025–Present

Dr. Ray Sedwick
Direct Energy Conversion
U. of Maryland · 2025

OPERATIONS

Michael Laughlin
Chief Operating Officer
2022–Present

Martin Owens
Chief Strategy Officer
LANL / GE Hitachi · 2022–Present

MG (Ret.) Paul Pardew
Chief Contracting Officer
Army Contracting Command · 2022–Present

David Beck
Fusion Commercialization
U.S. Space Force · 2024–Present

Sushma Bhatia
Environmental & Legislative
Google · 2022–Present

Michael De Frenza
Technology Licensing
2023–Present

MG (Ret.) Robin L. Fontes
Cybersecurity & Defense
Army Cyber Command · 2022–Present

Vijay Gehani
Supply Chain & Components
INOX India · 2024–Present

Jon Michel Greenwood
IT & AI Infrastructure
Live Nation · 2023–Present

Brian C. O'Neill
National Security
CIA / ODNI · 2022–Present

Gen. (Ret.) Gustave F. Perna
DoD Liaison
Operation Warp Speed · 2022–2023

Andrea Romero
Marketing Lead
2022–Present

Legal counsel is retained; those roles are held on the internal roster and are not listed here.

SOURCES

References

1 J E Menard *et al*, Fusion nuclear science facilities and pilot plants based on the spherical tokamak, *Nucl. Fusion* **56** 106023 (2016). doi:10.1088/0029-5515/56/10/106023

2 B N Sorbom *et al*, ARC: a compact, high-field, fusion nuclear science facility and demonstration power plant with demountable magnets, *Fusion Eng. Des.* **100** 378 (2015). doi:10.1016/j.fusengdes.2015.07.008

3 M E Austin *et al*, Achievement of reactor-relevant performance in negative triangularity shape in the DIII-D tokamak, *Phys. Rev. Lett.* **122** 115001 (2019). doi:10.1103/PhysRevLett.122.115001

4 A Marinoni, O Sauter and S Coda, A brief history of negative triangularity tokamak plasmas, *Rev. Mod. Plasma Phys.* **5** 6 (2021). doi:10.1007/s41614-021-00054-0

5 Y Camenen *et al*, Impact of plasma triangularity and collisionality on electron heat transport in TCV L-mode plasmas, *Nucl. Fusion* **47** 510 (2007).

6 A O Nelson *et al*, Robust avoidance of edge-localized modes alongside gradient formation in the negative triangularity tokamak edge, *Phys. Rev. Lett.* **131** 195101 (2023).

7 G Merlo *et al*, Nonlinear gyrokinetic simulations of negative-triangularity TCV discharges, *Plasma Phys. Control. Fusion* **61** 034001 (2019).

8 G M Staebler, J E Kinsey and R E Waltz, A theory-based transport model with comprehensive physics, *Phys. Plasmas* **14** 055909 (2007). doi:10.1063/1.2436852

9 J E Kinsey, G M Staebler and R E Waltz, The first transport code simulations using the trapped gyro-Landau-fluid model, *Phys. Plasmas* **15** 055908 (2008).

10 J Candy, E A Belli and R V Bravenec, A high-accuracy Eulerian gyrokinetic solver for collisional plasmas, *J. Comput. Phys.* **324** 73 (2016). doi:10.1016/j.jcp.2016.07.039

11 J Candy and R E Waltz, An Eulerian gyrokinetic-Maxwell solver, *J. Comput. Phys.* **186** 545 (2003). doi:10.1016/S0021-9991(03)00079-2

12 J Candy, C Holland, R E Waltz, M R Fahey and E Belli, Tokamak profile prediction using direct gyrokinetic and neoclassical simulation, *Phys. Plasmas* **16** 060704 (2009).

13 E A Belli and J Candy, Kinetic calculation of neoclassical transport including self-consistent electron and impurity dynamics, *Plasma Phys. Control. Fusion* **50** 095010 (2008).

14 H Sugama, T-H Watanabe and M Nunami, Linearized model collision operators for multiple ion species plasmas and gyrokinetic entropy balance equations, *Phys. Plasmas* **16** 112503 (2009).

15 R L Miller, M S Chu, J M Greene, Y R Lin-Liu and R E Waltz, Noncircular, finite aspect ratio, local equilibrium model, *Phys. Plasmas* **5** 973 (1998).

16 R E Waltz and R L Miller, Ion temperature gradient turbulence simulations and plasma flux surface shape, *Phys. Plasmas* **6** 4265 (1999).

17 A M Dimits *et al*, Comparisons and physics basis of tokamak transport models and turbulence simulations, *Phys. Plasmas* **7** 969 (2000).

18 R V Bravenec, J Candy, M Barnes and C Holland, Linear and nonlinear verification of gyrokinetic microstability codes, *Phys. Plasmas* **18** 122505 (2011).

19 M Greenwald, Verification and validation for magnetic fusion, *Phys. Plasmas* **17** 058101 (2010).

20 P W Terry *et al*, Validation in fusion research: towards guidelines and best practices, *Phys. Plasmas* **15** 062503 (2008).

21 F Jenko, W Dorland, M Kotschenreuther and B N Rogers, Electron temperature gradient driven turbulence, *Phys. Plasmas* **7** 1904 (2000). doi:10.1063/1.874014

22 K L van de Plassche, J Citrin, C Bourdelle *et al*, Fast modeling of turbulent transport in fusion plasmas using neural networks, *Phys.*

COLOPHON

How this document was made

The Kronos Fleet — Combined Editorial, 2026 is set in **Fraunces** (display), **Gelasio** (text), and **IBM Plex Mono** (data & equations), carried forward from the Kronos editorial design system.

The figures are rendered at 300 dpi from the deposited generator scripts; the document is composed as a single self-contained file with embedded fonts and imagery, paginated to US Letter, and rendered to PDF through a headless Chromium engine in matched light and dark editions.

Every headline quantity carries an evidence class; withdrawn and restated values are marked as such. Nothing herein is frozen beyond the founder-approved Tier-A set.

Explore it live — turn the interactive 3-D model, run the deposited solvers in the physics validator, and watch the companion film series.

◆

LEGAL NOTICE

Notice, status, and distribution

Conceptual design & simulation study. This document reports a conceptual design and simulation study. It is not a construction commitment, a safety-analysis report, a regulatory filing, or an offer of securities. Forward-looking statements — schedules, costs, market sizes, and performance — are estimates subject to the limitations set out in the Simulations part and may change.

Numbers and their classes. Quantities are reported with evidence classes and case labels; modelled, assumed, and requirement-class values are identified as such and are not to be quoted without their labels.

Public edition. This edition carries the physics and design only; all financial, funding, and defense-commercial content has been removed for public distribution. The scientific text corresponds to the arXiv and journal submissions.

THE 2026 KRONOS SERIES

One programme, many papers

This editorial is one paper in the Kronos 2026 series — a real fusion company's complete, reproducible physics record for a spherical-tokamak breeder and its low-neutron D–^{3}He tandem-mirror burners. Every headline number is a frozen anchor in the Physics De-Risking Register.

Explore the whole programme: the De-Risking Register, the interactive 3-D model, and the physics validator.

KRONOS FUSION ENERGY

Two-Code Cross-Validation of Negative-Triangularity Turbulence Suppression in a Compact Spherical-Tokamak Breeder: Quasilinear TGLF Confirms Nonlinear CGYRO

A real fusion company building real machines. Explore the science, live.

Zenodo · doi:10.5281/zenodo.22645864

Read on kronosfusionenergy.com

The Physics De-Risking Register